J. Fluid Mech. (1991), vol. 222, pp. 543–563
Printed in Great Britain

Film evaporation of a spherical droplet over a hot surface: fluid mechanics and heat/mass transfer analysis

By S. ZHANG AND G. GOGOS†

Department of Mechanical and Aerospace Engineering, Rutgers University, P.O. Box 909, Piscatway, NJ 08855-0909, USA

(Received 3 October 1989 and in revised form 17 April 1990)

Film evaporation of a spherical droplet over a hot surface is investigated in this paper. In view of the radial evaporation-induced velocity at the liquid–gas interface, an improvement over the classical flow field solution of Stimson & Jeffery (1926) needs to be employed. In addition to the flow, the energy equation internally and externally to the droplet and the species equation in the gas phase are also solved. The boundary conditions at the droplet surface couple the temperature, species and flow field. Analytical expressions for the hydrodynamic force and its components (viscous and pressure) that the droplet experiences are obtained. It is shown that, depending on the droplet separation distance from the hot surface and the type of liquid, there may be a substantial temperature variation along the droplet surface. Furthermore, considering a quasi-steady approximation for the droplet regression rate and balancing at each time step the weight of the droplet with the hydrodynamic force it experiences, time histories are obtained numerically for various quantities of interest. Thus, it is predicted that the droplet moves away from the hot surface while evaporating and that the initially substantial temperature variation along the droplet surface decreases with time and diminishes towards the end of the droplet lifetime. It is also shown that the droplet surface temperature is more uniform at higher hot-surface temperature.

1. Introduction

The understanding of droplet evaporation near a hot surface is of interest in many industrial applications such as combustion engines, turbine machinery and cooling and drying processes. A droplet evaporating over a hot surface undergoes different modes depending on the hot-surface temperature T_w. For T_w larger than the temperature corresponding to the so-called Leidenfrost point, the droplet evaporates while floating above its own vapour, and the evaporation time decreases with increasing T_w. This mode is called film evaporation. In this study, we investigated the fluid mechanics and heat/mass transfer of a droplet undergoing film evaporation.

A number of experimental and theoretical studies relevant to droplet film evaporation have appeared in the literature. Tamura & Tanasawa (1959) investigated the problem experimentally and presented a detailed description of the different modes of evaporation. The authors provide droplet evaporation time *vs.* hot-surface temperature for several pure and blended fuels. Gottfried, Lee & Bell (1966) and Gottfried & Bell (1966) measured the total evaporation time of a droplet for different initial droplet diameters (2–5 mm), different compounds (water, benzene,

† To whom correspondence should be addressed.

ethanol and n-octane), and different surface temperatures. The droplet lifetime and the droplet regression rate were measured. Furthermore, the authors provide a semi-empirical model of the evaporation process. The main assumptions employed are: (i) the flow is in a channel which is very narrow compared to its length to model the vapour flow between the droplet and the hot surface; (ii) heat is transferred to the droplet surface by conduction and radiation in the lower half and by radiation only in the upper half; (iii) quasi-steady vapour flow; and (iv) spatially uniform but temporally changing droplet temperature. A reasonable agreement with experiment was achieved. Following Gottfried *et al.* many studies extended their model in order to investigate more complicated problems. Avedisian & Koplik (1987) expanded the Gottfried model for a droplet evaporating over a porous surface. An analysis of flow in a horizontal channel bounded by an impermeable wall above (droplet surface) and a permeable wall of finite thickness below was used to model film evaporation. The model provided a basis for correlating droplet evaporation time measurements. The evaporation time decreased with increasing surface porosity at the same surface temperature. Avedisian, Ioffredo & O'Connor (1984) studied the effect of coal on the evaporation of water from mixtures of coal and water. Results showed that evaporation times of water were lower in the presence of coal than for a pure water droplet containing the same volume of water as in the corresponding coal/water mixture. Michiyoshi & Makino (1977) investigated the surface material effect (copper, brass, carbon steel and stainless steel) on the droplet evaporation time. For a fixed surface temperature above the Leidenfrost point, the same evaporation time was measured regardless of the kind of surface material. Presumably, the vapour film acts as a 'buffer zone' minimizing the effect of different surface material.

A careful examination of the experimental literature reveals that there is a difficulty with horizontal stability. Thus, Gottfried *et al.* (1966) report that, '...if the droplet wandered off the test surface the run was rejected'. Nevertheless, they were able to measure droplet lifetimes as a function of the hot-surface temperature and droplet radii as a function of time. Most of the other researchers referred to above resolved this difficulty by placing the droplet on a slightly concave surface.

With respect to theoretical work, Nguyen & Avedisian (1987) developed a numerical model using bispherical coordinates. The inertial terms for mass, heat and fluid flow were retained. However, the droplet temperature was assumed spatially uniform. It was predicted that evaporation time decreases with increasing surface temperature and that the droplet moves away from the surface as it evaporates. Sen & Law (1984) pursued a rigorous analytical solution in bispherical coordinates for a droplet evaporating near a hot plate. Their solution is given in an incomplete Gegenbauer series. In view of this it cannot describe a radially outward evaporation-induced velocity. It was predicted that the force on a droplet of a given radius increases as the droplet gets closer to the plate. Their solution is similar to that published for a pair of spheres moving in an unbounded ambience and separated by a given distance. Stimson & Jeffery (1926) obtained the flow-field solution for two solid spheres moving with equal small constant velocities parallel to their line of centres. Following their work, a number of studies were conducted to expand the Stimson & Jeffery solution. Goldman, Cox & Brenner (1966) determined the terminal settling motion of two spheres at small Reynolds numbers in an unbounded fluid. The authors obtained numerical values for the linear and angular velocities of the spheres as a function of their relative separation and of the orientation of their line-of-centres relative to the direction of gravity. They obtained good agreement with experimental data available in the literature. Haber, Hetsroni & Solan (1973) derived

exact solutions for the quasi-steady creeping flow internal and external to two droplets moving along their line of centres. Sadhal & Oguz (1985) investigated the translatory motion of a compound multiphase drop, consisting of a liquid drop or a gas bubble completely coated by another liquid, and moving in a third immiscible fluid. Its motion was investigated purely from a fluid-mechanics point of view. Oguz & Sadhal (1987) examined the time history of the motion of a compound multiphase drop undergoing growth or collapse due to change of phase in immiscible liquids. The incorporation of change of phase required the treatment of heat transfer along with the fluid mechanics.

With the exception of Oguz & Sadhal (1987), the above theoretical studies do not allow for normal velocity at the interface. The general flow-field solution presented in this study accounts for radially outward evaporation-induced velocity at the liquid–gas interfaces. It can be employed in solving the problem of a pair of interacting droplets moving in tandem in the Stokes' regime while undergoing evaporation. In this study it was utilized to solve the droplet film-evaporation problem. In addition to the flow, the energy equation internally and externally to the droplet and the species equation in the gas phase were also solved. The boundary conditions at the droplet interface couple the temperature, species and flow field. Results are presented for water and *n*-heptane (more volatile than water) droplets of 50, 100 and 150 μm in diameter. The hydrodynamic force that the droplet experiences, the hydrodynamic force components (viscous and pressure), the non-uniformity in the evaporation-induced velocity at the droplet surface, the droplet lifetime, the role played by the volatility of the type of liquid and the variation of the temperature along the droplet surface are predicted.

2. Theoretical formulation

Consider a single-component liquid droplet of radius R evaporating over a hot surface at temperature T_w in an inert environment (figure 1). The centre of the droplet is at a distance H from the hot surface and the closest point of the droplet to the hot surface is at a distance δ. The droplet is at its wet-bulb temperature and spatial temperature variation along the surface of the droplet and its interior is allowed.

The following assumptions are employed:

(i) The vapour flow field around the droplet is in the Stokes regime. The evaporation-induced velocity in the lower surface of the droplet is given by

$$V_{\text{evap}} \sim \frac{\lambda_g \Delta T}{\delta \rho_g h_{fg}},$$

where ΔT is the temperature difference between the droplet surface and the hot surface, λ_g and ρ_g are the thermal conductivity and density of the gaseous phase respectively, and h_{fg} is the heat of vaporization of the liquid droplet. For $\delta/R \ll 1$, the flow between the droplet and the hot surface can be considered as approximating channel flow. Then, the characteristic velocity for the flow is the radial velocity $V^* \sim (R/\delta)\, V_{\text{evap}}$. Consequently, the Reynolds number Re, that governs the flow regime is given by

$$Re = \left(\frac{\lambda_g \Delta T}{\mu_g h_{fg}}\right)\left(\frac{R}{\delta}\right),$$

where μ_g is the dynamic viscosity of the gaseous phase. Sufficiently small droplets can

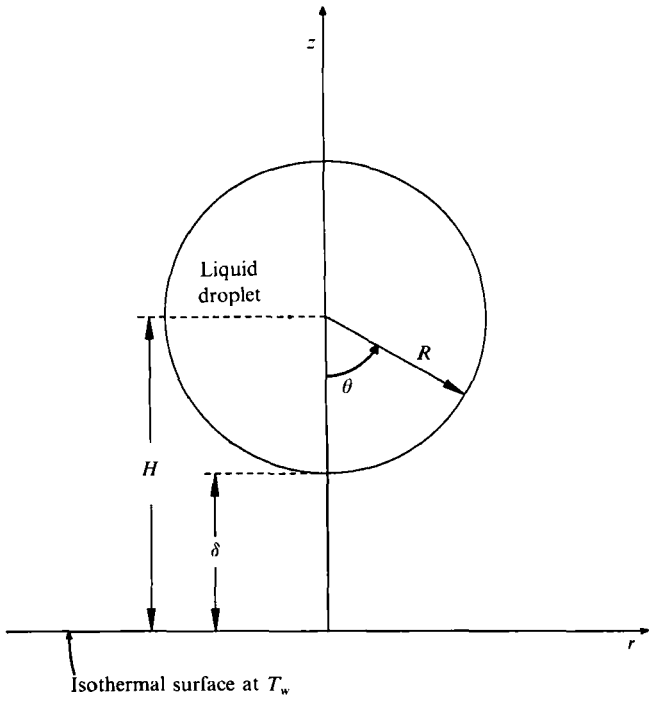

FIGURE 1. Geometry of the problem.

soar above the surface at a height comparable with their radius (Goldshtik, Khanin & Ligai 1986). It is with this case that the present study is concerned. Since $R/\delta \sim O(1)$, the Reynolds number $Re = \lambda_g \Delta T/\mu_g h_{fg}$. For water drops under normal conditions, $Re \approx 1$ only at $\Delta T \approx 1500$ K. For other substances, such as n-heptane and other hydrocarbons, the Reynolds number is small only for moderate temperature differences ($\Delta T < 200$ K).

(ii) Gas-phase quasi-steadiness. Owing to the significant density difference between the liquid and gas, quantities at the droplet surface such as regression rate, temperature and species concentration change at rates much slower than those of the gas-phase transport processes. Therefore, the gas-phase processes can be considered as steady (Law 1982).

(iii) Internal liquid motion is neglected. The neglect of any internal circulation within the droplet is justified on the basis of the small viscosity of the gaseous phase relative to that of the liquid.

(iv) Droplet shape remains spherical. The size of droplets typically found in industrial sprays are generally less than 150 μm in diameter. Thus, the droplet shape is considered spherical since the Eötvös number is very small.

(v) Radiation is negligible. Since $\sigma\epsilon(T_w^4 - T_b^4)/(\lambda_g(T_w - T_b)/\delta) \ll 1$, unless the hot-surface temperature is extremely high, radiation may be neglected. In the above expression σ is the Stefan–Boltzmann constant, ϵ is the gas emissivity and T_b is the boiling temperature of the liquid droplet.

(vi) Physical properties are constant.

With these approximations, we write the governing equations as follows.

For the gaseous phase:

$$\nabla \cdot \boldsymbol{V}_g = 0, \tag{2.1}$$

$$-\nabla p_g + \mu_g \nabla^2 \boldsymbol{V}_g = 0, \tag{2.2}$$

$$\nabla^2 T_g = 0, \tag{2.3}$$

$$\nabla^2 Y_g = 0, \tag{2.4}$$

For the liquid phase: $$\nabla^2 T_l = 0, \tag{2.5}$$

where g, l refer to gaseous and liquid phases respectively. In the above equations V is the velocity, T is the temperature, Y is the mass fraction of the vaporizing species and p is the pressure.

The boundary conditions are

On the hot surface: $$V_g = 0, \tag{2.6}$$

$$T_g = T_w, \tag{2.7}$$

$$\frac{\partial Y_g}{\partial n} = 0. \tag{2.8}$$

On the droplet surface: $$V_{g\tau} = 0, \tag{2.9}$$

$$T_g = T_l \tag{2.10}$$

$$(1-Y_g)\, V_{gn} + D_g \frac{\partial Y_g}{\partial n} = 0 \quad \text{(impermeability condition)}, \tag{2.11}$$

$$\lambda_g \frac{\partial T_g}{\partial n} - \lambda_l \frac{\partial T_l}{\partial n} = \rho_g V_{gn} h_{fg} \quad \text{(interfacial heat balance)}, \tag{2.12}$$

$$Y_g = \frac{\gamma \exp\left[\dfrac{h_{fg}}{R^0}\left(\dfrac{1}{T_b} - \dfrac{1}{T_g}\right)\right]}{1-(1-\gamma)\exp\left[\dfrac{h_{fg}}{R^0}\left(\dfrac{1}{T_b} - \dfrac{1}{T_g}\right)\right]} \quad \text{(Clausius–Clapeyron equation)}, \tag{2.13}$$

where γ = molecular weight of vapour/molecular weight of inert gas, subscripts n and τ indicate normal and tangential directions respectively, R^0 is the universal gas constant and D_g is the binary gas diffusion coefficient. Furthermore, the temperature remains finite everywhere in the droplet interior and far away from the droplet, $T_g = T_w$ and $Y_g = 0$.

Note that the system of equations is nonlinear owing to the coupling of T_g, Y_g and V_{gn} in the Clausius–Clapeyron equation and impermeability condition. The governing equations in dimensionless form are as follows:

$$\nabla' \cdot V'_g = 0, \tag{2.14}$$

$$-\nabla' p'_g + \nabla'^2 V'_g = 0, \tag{2.15}$$

$$\nabla'^2 T'_g = 0, \tag{2.16}$$

$$\nabla'^2 Y_g = 0, \tag{2.17}$$

$$\nabla'^2 T'_l = 0. \tag{2.18}$$

Boundary conditions:

on the hot surface $$V'_g = 0, \tag{2.19}$$

$$T'_g = 0, \tag{2.20}$$

$$\frac{\partial Y_g}{\partial n'} = 0; \tag{2.21}$$

on the droplet surface

$$V'_{g\tau} = 0, \tag{2.22}$$

$$T'_g = T'_l. \tag{2.23}$$

Combining (2.11) and (2.12)

$$w_g \frac{\partial T'_g}{\partial n'} - w_l \frac{\partial T'_l}{\partial n'} = -\frac{1}{1-Y_g} \frac{\partial Y_g}{\partial n'}. \tag{2.24}$$

Furthermore, the Clausius–Clapeyron equation is given by (2.13). In the above equations

$$w_g = \frac{\lambda_g \Delta T}{\rho_g D_g h_{fg}}, \quad w_l = \frac{\lambda_l}{\lambda_g} w_g, \quad T' = \frac{T - T_w}{\Delta T},$$

$$V' = \frac{V}{V^*}, \quad \nabla' = L^* \nabla, \quad \delta' = \frac{\delta}{L^*}, \quad p'_g = \frac{p_g}{p_g^*}.$$

The asterisk indicates the characteristic quantities which have been chosen as

$$L^* = D, \quad V^* = \lambda_g \Delta T / L^* \rho_g h_{fg}, \quad p_g^* = \mu_g V^* / L^*, \quad \Delta T = T_w - T_b,$$

where D is droplet diameter. For simplicity, we omit the prime hereafter. In the next section the analytical solution to the problem is derived.

3. Method of solution

The temperature field both in the gas and liquid phases and the gas-phase vapour mass fraction are obtained first. This part of the solution provides the wet-bulb temperature along the droplet surface and the radial evaporation-induced velocity at the droplet surface, which is then used as a boundary condition for the equations governing the flow field.

3.1. *Temperature and vapour mass fraction fields*

The solution is obtained in bispherical coordinates (ξ, η, ϕ). Owing to axisymmetry, the solution is independent of ϕ. The bispherical coordinates are related to the cylindrical coordinates (r, z, ϕ) through the transformations

$$z = \frac{c \sinh \xi}{\cosh \xi - \cos \eta}, \tag{3.1}$$

$$r = \frac{c \sin \eta}{\cosh \xi - \cos \eta}, \tag{3.2}$$

where $-\infty < \xi < \infty$, $0 \leqslant \eta \leqslant \pi$, and $c > 0$ is half the distance between the points defined by $\xi \to \infty$ and $\xi \to -\infty$ on the z-axis. Choosing $H = c \coth \beta$ and $R = c/\sinh \beta$ would let the droplet surface and the hot surface to be represented by coordinates of constant values, $\xi = \beta$ and $\xi = 0$ respectively, so that the method of separation of variables can be employed.

Initially equations (2.13) and (2.24) are replaced by the following expansions:

$$T_g|_{\xi=\beta} = (\cosh \beta - \mu)^{\frac{1}{2}} \sum_{n=0}^{\infty} c_n P_n(\mu), \tag{3.3}$$

$$Y_g|_{\xi=\beta} = (\cosh \beta - \mu)^{\frac{1}{2}} \sum_{n=0}^{\infty} d_n P_n(\mu), \tag{3.4}$$

where $P_n(\mu)$ is Legendre polynomial of order n and $\mu = \cos\eta$. Using (3.3) and (3.4) together with the boundary conditions as provided by (2.20), (2.21) and (2.23) as well as finiteness at the droplet interior ($T_l|_{\xi\to\infty} < \infty$), the solutions to (2.16)–(2.18) are obtained as

$$T_g = (\cosh\xi - \mu)^{\frac{1}{2}} \sum_{n=0}^{\infty} c_n \frac{\sinh(n+\frac{1}{2})\xi}{\sinh(n+\frac{1}{2})\beta} P_n(\mu), \tag{3.5}$$

$$Y_g = (\cosh\xi - \mu)^{\frac{1}{2}} \sum_{n=0}^{\infty} d_n \frac{\cosh(n+\frac{1}{2})\xi}{\cosh(n+\frac{1}{2})\beta} P_n(\mu), \tag{3.6}$$

$$T_l = (\cosh\xi - \mu)^{\frac{1}{2}} \sum_{n=0}^{\infty} c_n \mathrm{e}^{-(n+\frac{1}{2})(\xi-\beta)} P_n(\mu). \tag{3.7}$$

The above solutions satisfy $Y_g = 0$ and $T_g = T_w$ at infinity ($\xi \to 0, \mu = 1$). The Clausius–Clapeyron equation and (2.24), which was obtained by combining the impermeability condition and the interfacial heat balance at the droplet surface, are used next to solve for c_n and d_n. The Clausius–Clapeyron equation can be linearized about some reference temperature T_{ref} as

$$Y_g = a + bT_g, \tag{3.8}$$

where

$$a = \frac{\gamma \exp\left[\frac{h_{fg}}{R^0}\left(\frac{1}{T_b} - \frac{1}{T_{ref}}\right)\right]}{1-(1-\gamma)\exp\left[\frac{h_{fg}}{R^0}\left(\frac{1}{T_b} - \frac{1}{T_{ref}}\right)\right]} \left\{1 + \frac{h_{fg}(T_w - T_{ref})}{R^0 T_{ref}^2 \left\{1-(1-\gamma)\exp\left[\frac{h_{fg}}{R^0}\left(\frac{1}{T_b} - \frac{1}{T_{ref}}\right)\right]\right\}}\right\} \tag{3.9}$$

and

$$b = \frac{\gamma h_{fg} \Delta T \exp\left[\frac{h_{fg}}{R^0}\left(\frac{1}{T_b} - \frac{1}{T_{ref}}\right)\right]}{R^0 T_{ref}^2 \left\{1-(1-\gamma)\exp\left[\frac{h_{fg}}{R^0}\left(\frac{1}{T_b} - \frac{1}{T_{ref}}\right)\right]\right\}^2}. \tag{3.10}$$

Combining (3.5), (3.6) and (3.8):

$$d_n = bc_n + \sqrt{2}a\,\mathrm{e}^{-(n+\frac{1}{2})\beta}, \quad n = 0, 1, \ldots \tag{3.11}$$

Combining (2.24) and (3.5)–(3.7), we obtain

$$\sum_{m=0}^{\infty}\left\{Q_m \sum_{n=0}^{m-1} N_{lmn}\sqrt{2}\,\mathrm{e}^{-(n+\frac{1}{2})\beta} - G_m \sum_{n=0}^{m-1} N_{lmn} d_n + \sum_{n=0}^{m} N_{lmn}(\sqrt{2}\,\mathrm{e}^{-(m+\frac{1}{2})\beta} Q_n - d_m G_n)\right\}$$
$$= -\sum_{m=0}^{\infty}\left\{\sum_{n=0}^{m}(\sqrt{2}\,\mathrm{e}^{-(m+\frac{1}{2})\beta} R_n + \sqrt{2}\,\mathrm{e}^{-(n+\frac{1}{2})\beta} R_m) N_{lmn} - N_{lmn}\sqrt{2}\,\mathrm{e}^{-(m+\frac{1}{2})\beta} R_m\right\},$$
$$l = 0, 1, \ldots, \tag{3.12}$$

where

$$\begin{aligned}
Q_n &= c_n\{(w_g - w_1 + b)\sinh\beta + (2n+1)[w_g \coth(n+\tfrac{1}{2})\beta + w_g \\
&\quad + b\tanh(n+\tfrac{1}{2})\beta]\cosh\beta\} - nc_{n-1}\{w_g\coth(n-\tfrac{1}{2})\beta + w_1 + b\tanh(n-\tfrac{1}{2})\beta\} \\
&\quad - (n+1)c_{n+1}\{w_g\coth(n+\tfrac{3}{2})\beta + w_1 + b\tanh(n+\tfrac{3}{2})\beta\}, \\
R_n &= \sqrt{2}\,a\{\mathrm{e}^{-(n+\frac{1}{2})\beta}[\sinh\beta + (2n+1)\cosh\beta\tanh(n+\tfrac{1}{2})\beta] \\
&\quad - n\,\mathrm{e}^{-(n-\frac{1}{2})\beta}\tanh(n-\tfrac{1}{2})\beta - (n+1)\,\mathrm{e}^{-(n+\frac{3}{2})\beta}\tanh(n+\tfrac{3}{2})\beta\}, \\
G_n &= c_n\{(w_g - w_1)\sinh\beta + (2n+1)[w_g\coth(n+\tfrac{1}{2})\beta + w_1]\cosh\beta\} \\
&\quad - nc_{n-1}[w_g\coth(n+\tfrac{3}{2})\beta + w_1] - (n+1)c_{n+1}[w_g\coth(n+\tfrac{3}{2})\beta + w_1]
\end{aligned}$$

and $$N_{lmn} = \int_{-1}^{1} P_l(\mu) P_m(\mu) P_n(\mu) \, \mathrm{d}\mu. \tag{3.13}$$

The integral in (3.13) results from (2.24). Since the solutions to T_g, T_l and Y_g are expressed as series of Legendre polynomials, the appearance of the term $1 - Y_g$ on the right-hand side of (2.24) leads to a product of such series. Expressing this product as a single series of Legendre polynomials introduces the integral given by (3.13). The evaluation of this integral is given by Gaunt (1929).

The solution to (3.11) and (3.12) provides c_n and d_n. These two equations are solved iteratively, since (3.12) is nonlinear.

3.2. *Velocity field*

The governing equations and boundary conditions for the flow field are

$$\nabla \cdot \boldsymbol{V}_g = 0, \tag{3.14}$$

$$-\nabla p_g + \nabla^2 \boldsymbol{V}_g = 0; \tag{3.15}$$

on the plate $$\boldsymbol{V}_g = 0; \tag{3.16}$$

and on the droplet surface

$$\boldsymbol{V}_g = \frac{\partial \tilde{T}}{\partial n} \boldsymbol{n}, \tag{3.17}$$

where $\tilde{T} = T_g - \lambda T_l$ and $\lambda = \lambda_l / \lambda_g$. Note that the right-hand side of (3.17) is provided by the temperature-field solution obtained in §3.1. Introducing the stream function Ψ, the velocity components in bispherical coordinates are given by

$$V_\xi = \frac{(\cosh \xi - \mu)^2}{c^2 \sin \eta} \frac{\partial \Psi}{\partial \eta}, \tag{3.18}$$

$$V_\eta = -\frac{(\cosh \xi - \mu)^2}{c^2 \sin \eta} \frac{\partial \Psi}{\partial \xi}. \tag{3.19}$$

Then the momentum equation becomes

$$E^4 \Psi = 0, \tag{3.20}$$

where

$$E^2 = (\cosh \xi - \mu) \left\{ \frac{\partial}{\partial \xi} (\cosh \xi - \mu) \frac{\partial}{\partial \xi} + (1 - \mu^2) \frac{\partial}{\partial \mu} (\cosh \xi - \mu) \frac{\partial}{\partial \mu} \right\}. \tag{3.21}$$

On the plate ($\xi = 0$) $$\Psi = 0, \tag{3.22}$$

$$\frac{\partial \Psi}{\partial \xi} = 0, \tag{3.23}$$

and on the droplet surface ($\xi = \beta$)

$$\frac{\partial \Psi}{\partial \xi} = 0, \tag{3.24}$$

$$\frac{\partial \tilde{T}}{\partial \xi} = -\frac{(\cosh \beta - \mu)}{c} \frac{\partial \Psi}{\partial \mu}. \tag{3.25}$$

The general solution of (3.20) can be written as (Appendix A)

$$\Psi = (\cosh \xi - \mu)^{-\frac{3}{2}} \sum_{n=-1}^{\infty} F_n(\xi) \, C_{n+1}^{-\frac{1}{2}}(\mu), \tag{3.26}$$

where

$$F_n(\xi) = A_n \cosh(n-\tfrac{1}{2})\xi + B_n \sinh(n-\tfrac{1}{2})\xi + C_n \cosh(n+\tfrac{3}{2})\xi + D_n \sinh(n+\tfrac{3}{2})\xi, \tag{3.27}$$

and $C_{n+1}^{-\frac{1}{2}}(\mu)$ are Gegenbauer polynomials of order $(n+1)$ and degree $-\frac{1}{2}$.

Note that the stream-function series solution starts with $n = -1$. With the exception of Oguz & Sadhal (1987), the above solution appeared extensively in prior works starting with $n = 1$. This has been adequate since these works dealt with non-evaporating spheres. According to Sampson (1891), the expansion of Ψ requires a complete set of eigenfunctions whenever $\Psi|_{\mu=1} \neq \Psi|_{\mu=-1}$. In this problem, owing to the outward, evaporation-induced flow field $\Psi|_{\mu=1} \neq \Psi|_{\mu=-1}$, therefore it is critically important to keep the additional terms. Ensuring that the velocity components remain finite in the solution domain (Appendix A), the stream function is given by

$$\Psi = (\cosh\xi - \mu)^{-\frac{3}{2}}[Q(\xi,\mu) + \sum_{n=1}^{\infty} F_n(\xi)\, C_{n+1}^{-\frac{1}{2}}(\mu)], \tag{3.28}$$

where

$$Q(\xi,\mu) = A(1-\mu)[\cosh(\tfrac{1}{2}\xi) + \tfrac{1}{3}\cosh(\tfrac{3}{2}\xi)] + B(1+\mu)[\sinh(\tfrac{1}{2}\xi) - \tfrac{1}{3}\sinh(\tfrac{3}{2}\xi)]. \tag{3.29}$$

The integration constants A_n, B_n, C_n, D_n, A and B can be obtained by satisfying the boundary conditions, (3.22)–(3.25). Using boundary condition (3.22) and (3.23)

$$A = 0, \tag{3.30}$$

$$A_n + C_n = 0, \quad n = 1, 2, \ldots, \tag{3.31}$$

$$(2n-1)B_n + (2n+3)D_n = 0, \quad n = 1, 2, \ldots. \tag{3.32}$$

Using (3.31) and (3.32), we eliminate C_n and D_n. The remaining integration constants A_n, B_n and B can be obtained using boundary conditions (3.24) and (3.25). After some lengthy algebra a system of equations of order $2M+1$ is obtained (Appendix B), where M is the number of terms that need to be retained in the series solution for adequate accuracy. The system of equations can be put into a matrix form and are solved numerically. Once the flow-field solution is obtained, the evaporation rate, the hydrodynamic force that the droplet experiences, and other physical quantities of interest can be computed.

3.3. *Physical quantities*

In this section equations are presented in dimensional form for obtaining the hydrodynamic force and the droplet regression rate. The force, F, exerted on the liquid droplet is given by

$$F = F_\mu + F_p, \tag{3.33}$$

where the viscous component F_μ and pressure component F_p are

$$F_\mu = \int_s z \cdot (2\mu_g \hat{\boldsymbol{S}}) \cdot \mathrm{d}s \tag{3.34}$$

and

$$F_p = \int_s z \cdot (-p\hat{\boldsymbol{I}}) \cdot \mathrm{d}s. \tag{3.35}$$

In the above $\hat{\boldsymbol{S}} = \frac{1}{2}[\nabla V + (\nabla V)^{\mathrm{T}}]$ and $\mathrm{d}s$ is a surface element on the droplet surface. Introducing the stream function Ψ, the force components in bispherical coordinates are given by

$$F_\mu = -\frac{2\pi\mu_g \sinh\beta}{c} \int_{-1}^{1} \frac{1}{(\cosh\beta - \mu)^2} E^2 \Psi \, \mathrm{d}\mu \tag{3.36}$$

and
$$F_p = -\frac{\mu_g \pi}{c} \int_{-1}^{1} \frac{1}{\cosh\beta - \mu} \left.\frac{\partial E^2 \Psi}{\partial \xi}\right|_{\xi=\beta} \mathrm{d}\mu. \tag{3.37}$$

Substituting the solution for Ψ in (3.36) and (3.37), the following formulae for the viscous and pressure components were obtained after some extremely tedious algebra:

$$\begin{aligned} F_\mu = {} & \frac{32\sqrt{2}}{9} \frac{\pi\mu_g}{c} \mathrm{e}^{-\beta/2} \sinh\tfrac{1}{2}\beta \sinh\beta (\coth\beta - 1)(2\cosh\beta + 1) B \\ & - \frac{16\sqrt{2}}{3} \frac{\pi\mu_g \sinh\beta}{c} \sum_{n=1}^{\infty} \left\{ \mathrm{e}^{-2\omega\beta} (2\omega \sinh\beta - 3\cosh\beta) A_n \right. \\ & \left. - \frac{1}{(\omega+1)} \mathrm{e}^{-\omega\beta} \left[\mathrm{e}^{-\omega\beta} (2\omega^2 \sinh\beta - \omega\cosh\beta - 3\sinh\beta) + \frac{\sinh\omega\beta}{\sinh\beta} \right] B_n \right\} \end{aligned} \tag{3.38}$$

and

$$\begin{aligned} F_p = {} & \frac{8\sqrt{2}}{3} \frac{\pi\mu_g}{c} \mathrm{e}^{-\beta/2} \sinh\beta \sinh\tfrac{1}{2}\beta (\coth\beta - 1) [\sinh\beta (\coth^2\beta - \tfrac{2}{3}\coth\beta + 1) \\ & + \coth\beta - \tfrac{1}{3}] B + \frac{16\sqrt{2}}{3} \frac{\pi\mu_g \sinh\beta}{c} \sum_{n=1}^{\infty} \left\{ \mathrm{e}^{-2\omega\beta} (2\omega \sinh\beta - 3\cosh\beta) A_n \right. \\ & + \frac{1}{\omega+1} \mathrm{e}^{-\omega\beta} \left[\mathrm{e}^{-\omega\beta} (-2\omega^2 \sinh\beta + \omega\cosh\beta + 3\sinh\beta) \right. \\ & \left. \left. + \frac{(3\cosh\omega\beta - \sinh\omega\beta)}{4\sinh\beta} \right] B_n \right\}, \end{aligned} \tag{3.39}$$

where $\omega = n + \frac{1}{2}$. The total hydrodynamic force is given by

$$F = \frac{8\sqrt{2}\mu_g \pi}{c} \left\{ \tfrac{1}{3} B + \sum_{n=1}^{\infty} \frac{B_n}{2n+3} \right\}. \tag{3.40}$$

The droplet regression rate is given by

$$\frac{\mathrm{d}m}{\mathrm{d}t} = -\rho_g \int_s V_{gn} \, \mathrm{d}s, \tag{3.41}$$

where m is the mass of the droplet and t is time. Furthermore, balancing the hydrodynamic force with the droplet weight we obtain

$$mg = F. \tag{3.42}$$

The contribution of the acceleration term, which was left out in the above equation, has been investigated. The term plays a role only towards the end of the droplet lifetime when $\mathrm{d}\delta/\mathrm{d}t$ changes at a faster rate (see figure 10), but it still remains negligible. Numerical integration of (3.41), while satisfying equation (3.42) at each time step, provides time histories for the separation distance between the droplet and the hot surface, the temperature field, the evaporation rate, and other physical quantities of interest.

4. Results and discussion

We now present results for water and n-heptane droplets evaporating in air. Computations have been carried out for hot-surface temperatures of 573, 673, 773 and 873 K for water droplets and 472 and 572 K for n-heptane droplets. The short

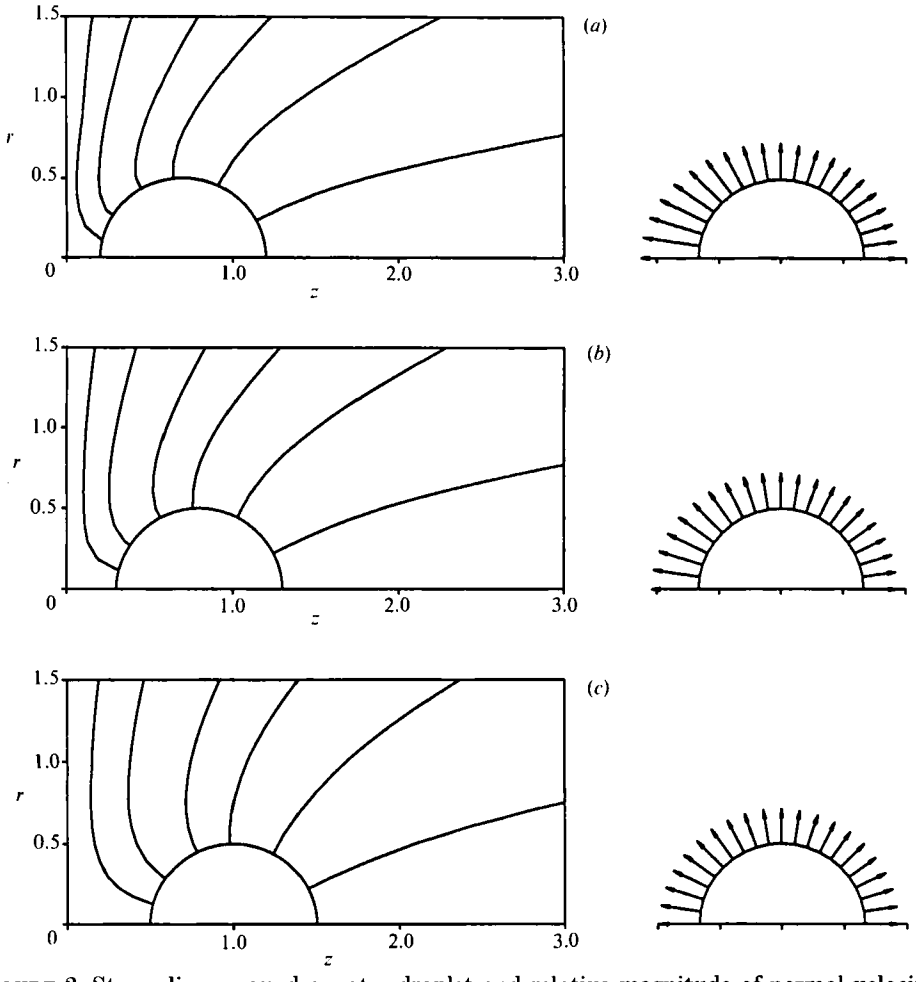

FIGURE 2. Streamlines around a water droplet and relative magnitude of normal velocity V_{gn} at the droplet surface for three different separation distances: (*a*) $\delta = 0.2$, (*b*) $\delta = 0.3$, (*c*) $\delta = 0.5$. ($T_w = 673$ K.)

range of surface temperatures chosen for the *n*-heptane cases is imposed by the small-Reynolds-number restriction of the theory presented above. Both substances have approximately the same boiling temperature ($T_b = 373.15$ K for water and $T_b = 371.55$ K for *n*-heptane). The two differ substantially in volatility, with the *n*-heptane being the more volatile.

In the first section below we present quasi-steady results for droplets located at fixed distances from the hot surface. In the second section, time histories are presented for droplets suspended on their own vapour while evaporating. Based on sphericity considerations, a droplet diameter of 100 μm was used, unless otherwise indicated. The physical properties were obtained from Raznjevic (1976) and Vargaftik (1975).

4.1. *Quasi-steady results*

In figure 2 the streamlines around the droplet and the corresponding magnitude of the normal velocity V_{gn} at the droplet surface are presented for three separation distances. The non-uniformity in V_{gn} caused by the hot surface is intense for small

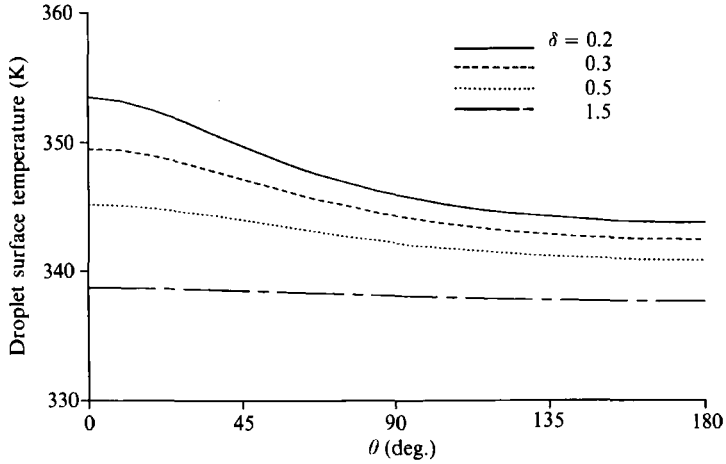

FIGURE 3. Effect of separation distance δ on the temperature variation along the droplet surface (water droplet, $T_w = 673$ K).

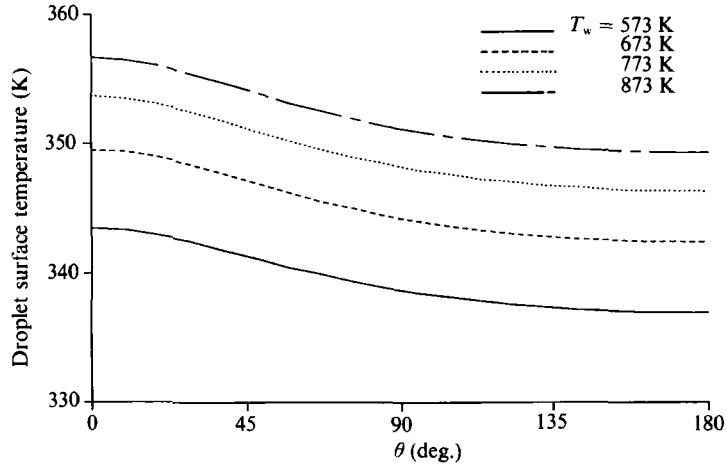

FIGURE 4. Effect of wall temperature T_w on the temperature variation along the droplet surface (water droplet, $\delta = 0.3$).

separation distances δ and weakens as δ increases. For a separation distance of one radius ($\delta = 0.5$), V_{gn} is almost uniform. In figure 3 the effect of separation distance on the temperature variation along the droplet surface for a water droplet is shown. For a separation distance of $\frac{2}{5}$ of the droplet radius ($\delta = 0.2$), the temperature difference between $\theta = 0$ and 180° is as much as 10 K. The linearization of the Clausius–Clapeyron equation within such a temperature range leads to a maximum error of 2%. This temperature difference weakens as δ increases. At a separation distance of three radii ($\delta = 1.5$) the droplet is at an almost uniform temperature. Approximately 80% of the temperature variation takes place on the droplet half facing the hot surface. Also, note that the droplet surface temperature is the so-called web-bulb temperature, which is substantially below the normal boiling point for water. Figure 4 presents the effect of the hot-surface temperature, T_w, on the temperature variation along the droplet surface for a water droplet. The droplet

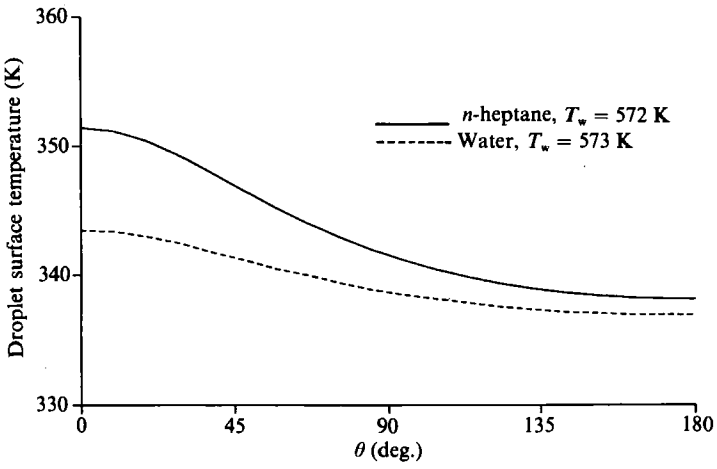

FIGURE 5. Effect of liquid type on the temperature variation along the droplet surface ($\delta = 0.3$).

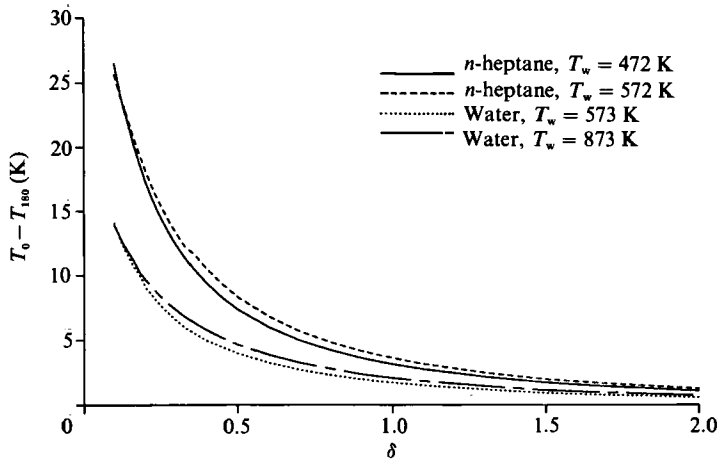

FIGURE 6. The variation of the droplet surface maximum temperature difference with δ, T_w and liquid type.

surface temperature is raised overall with increasing T_w; however, the temperature difference between $\theta = 0$ and 180° remains approximately the same for different values of T_w. In figure 5 the effect of liquid type on the temperature variation along the droplet surface is shown. The temperature variation along the surface for the water droplet is much smaller than that for an *n*-heptane droplet, since the thermal conductivity of water is approximately seven times that of *n*-heptane. The maximum difference in the droplet surface temperature between $\theta = 0$ and 180° ($T_0 - T_{180}$) is shown in figure 6 as a function of separation distance δ, for water and *n*-heptane droplets for various hot-surface temperatures.

The hydrodynamic force exerted on a water droplet is plotted in figure 7 as a function of separation distance for different hot-surface temperatures. The hydrodynamic force decreases asymptotically to zero with increasing δ. For the same value of δ, the hydrodynamic force increases with T_w, since the radially outward evaporation-induced flow field intensifies with increasing T_w. In figure 8 the

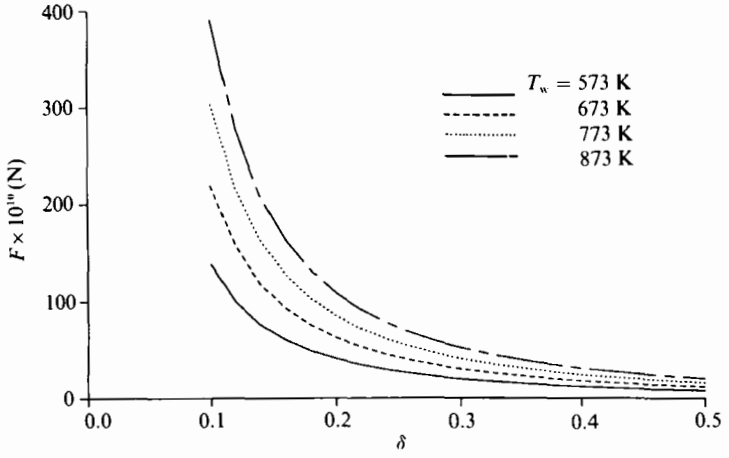

FIGURE 7. Variation of the hydrodynamic force on a water droplet with δ and T_w.

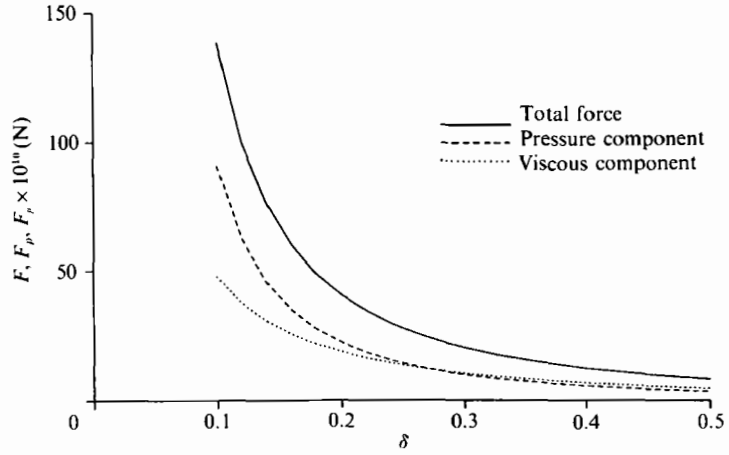

FIGURE 8. Variation of the hydrodynamic force and its components for a water droplet with δ (T_w = 573 K).

hydrodynamic force and its components are plotted as a function of separation distance for a water droplet. For small separation distances the pressure force component is significantly larger than the viscous force, whereas for large separation distances the two components are comparable. It is a common assumption in some early models constructed for the Leidenfrost problem that the weight of the droplet is balanced by the pressure force only (Gottfried & Bell 1966; Avedisian & Koplik 1987). The dominant role of F_p at small separation distances evidenced in the present analysis strongly supports that assumption. Figure 9 shows the hydrodynamic force and its components for an *n*-heptane droplet. Comparison with figure 8 reveals that the hydrodynamic force on the more volatile *n*-heptane droplet is larger than that exerted on the water droplet by a factor of approximately four.

4.2. *Transient results*

Time histories of physical quantities are obtained by balancing the weight of the droplet with the hydrodynamic force exerted on it at each time step. The droplet weight is updated at each time step using (3.41), which provides the droplet rate of

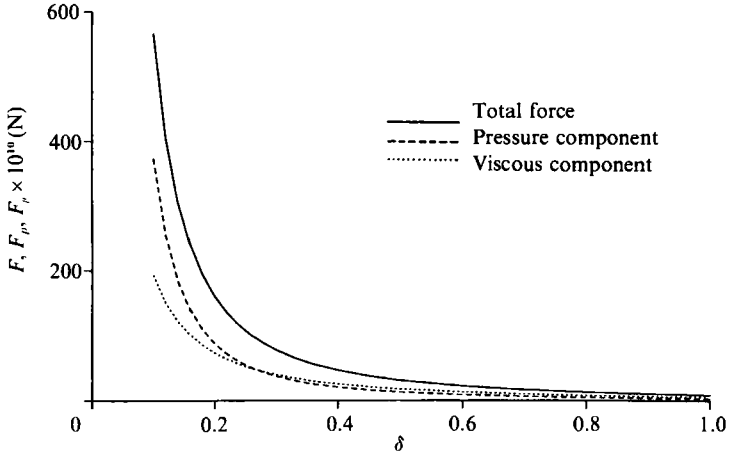

FIGURE 9. Variation of the hydrodynamic force and its components for an *n*-heptane droplet with δ ($T_w = 572$ K).

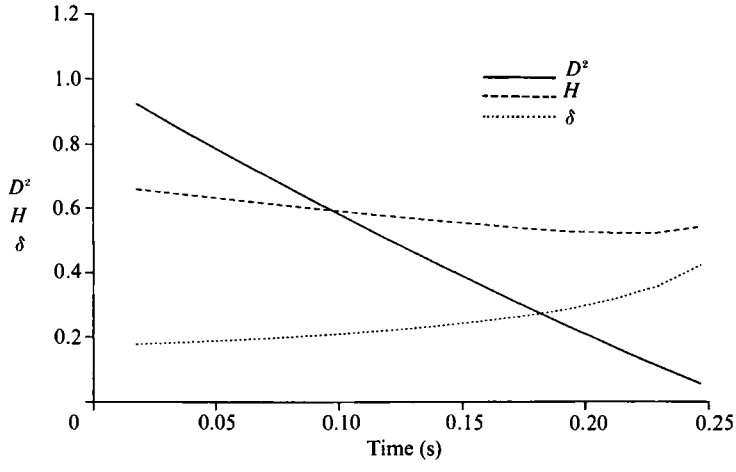

FIGURE 10. Temporal variation of the diameter squared (D^2), separation distance (δ) and distance of the droplet centre from the hot surface (H) for a water droplet ($T_w = 573$ K, $D_0 = 100$ μm).

regression. In figure 10 the square of the droplet diameter (D^2), the separation distance (δ) and the distance of the droplet centre from the hot surface (H) are shown as functions of time for a water droplet. The initial droplet diameter is used to make the above quantities dimensionless. The droplet appears to be moving away from the hot surface as was also predicted by Nguyen & Avedisian (1987). Direct comparison was not possible since the authors presented results using three different temperatures; plate, far-field and droplet surface temperature. The droplet centre moves downward; however, the regression of the droplet diameter is faster so that the separation distance δ increases. The droplet lifetime as a function of hot-surface temperature for different droplet initial diameters is provided in figure 11. The lifetime of the larger droplets decreases faster than that of the smaller droplets with increasing hot-surface temperature, which is in qualitative agreement with the experimental results of Tamura & Tanasawa (1959). In figure 12 the time histories

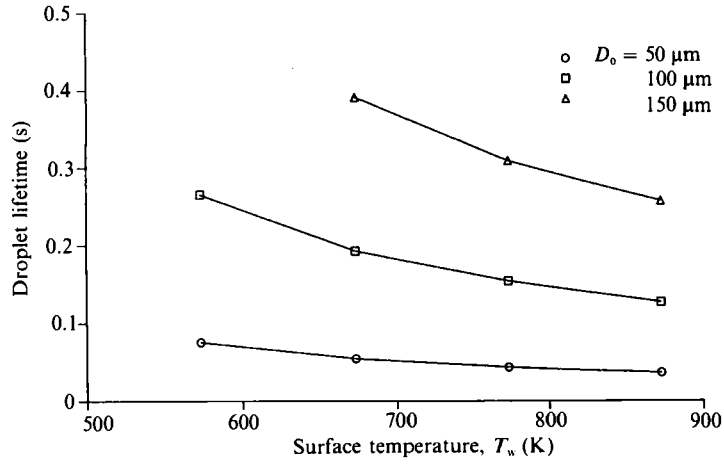

FIGURE 11. Droplet lifetime versus hot-surface temperature (water droplet) for various initial droplet diameters D_0.

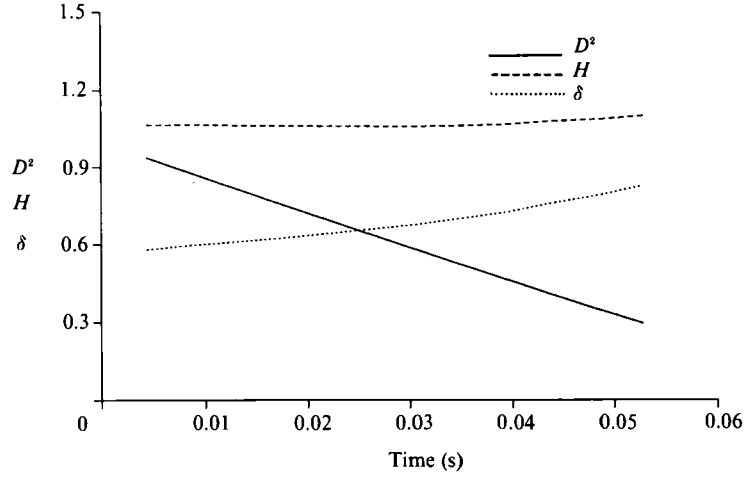

FIGURE 12. Temporal variation of the diameter squared (D^2), separation distance (δ) and distance of the droplet centre from the hot surface (H) for a water droplet (T_w = 573 K, D_0 = 50 μm).

of D^2, δ and H are plotted for a water droplet of initial diameter 50 μm. Comparison with figure 10 reveals that the smaller droplet remains at a much larger separation distance δ throughout its lifetime.

The temporal variations of D^2, δ and H are shown in figure 13 for an n-heptane droplet. Comparison with figure 10, for a water droplet, reveals that not only δ but also H increases with time. Furthermore, owing to the higher volatility of n-heptane, the flow field is much stronger so that much higher values for δ and H are predicted than those for a water droplet.

The temporal variation of the maximum temperature difference across the droplet surface $T_0 - T_{180}$ is shown in figure 14. $T_0 - T_{180}$ decreases monotonically with time as the size of the droplet decreases. Higher values of T_w lead to smaller $T_0 - T_{180}$, since δ increases with T_w; it was shown above (quasi-steady results) that $T_0 - T_{180}$ decreases with increasing δ (figure 3) and changes weakly with T_w (figure 6). In figure 15 the

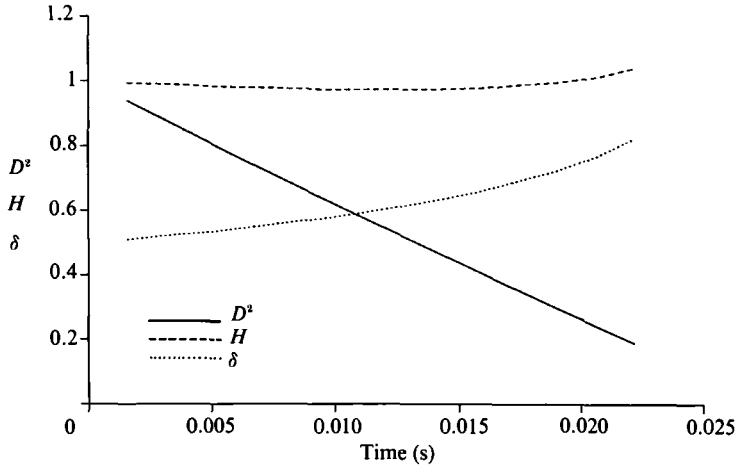

FIGURE 13. Temporal variation of the diameter squared (D^2), separation distance (δ) and distance of the droplet centre from the hot surface (H) for an n-heptane droplet ($T_w = 572$ K, $D_0 = 100$ μm).

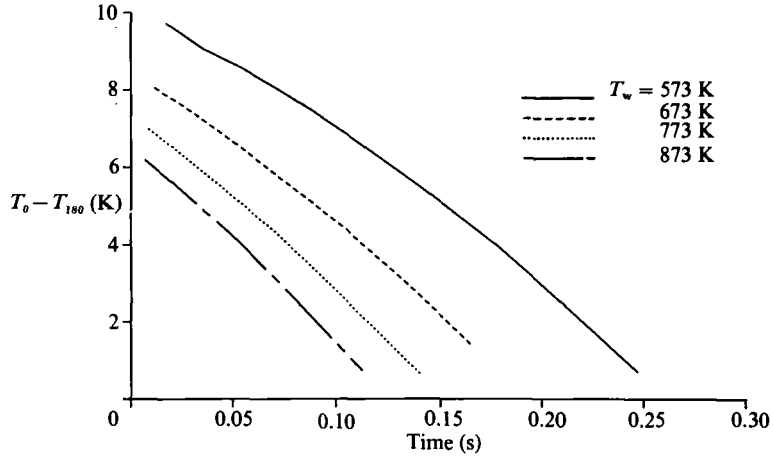

FIGURE 14. Temporal variation of the maximum temperature difference across the droplet surface for a water droplet with T_w ($D_0 = 100$ μm).

time histories of $T_0 - T_{180}$ for droplets of different initial diameters are shown. The temperature difference, $T_0 - T_{180}$, is much greater for larger droplets owing both to their size and the smaller separation distance δ. Therefore, in order to keep the error due to linearization of the Clausius–Clapeyron equation small, a limit is imposed on the size of droplet that can be considered.

5. Conclusion

In the present study we have carried out a detailed theoretical analysis of droplet film evaporation over a hot surface. The fluid mechanics and the heat/mass transfer involved have been carefully studied; the droplet lifetime, the non-uniformity in the temperature along the droplet surface, the separation distance between the droplet and the hot surface and the effect of the volatility of the liquid on the above quantities have been predicted and discussed. Results have been presented for

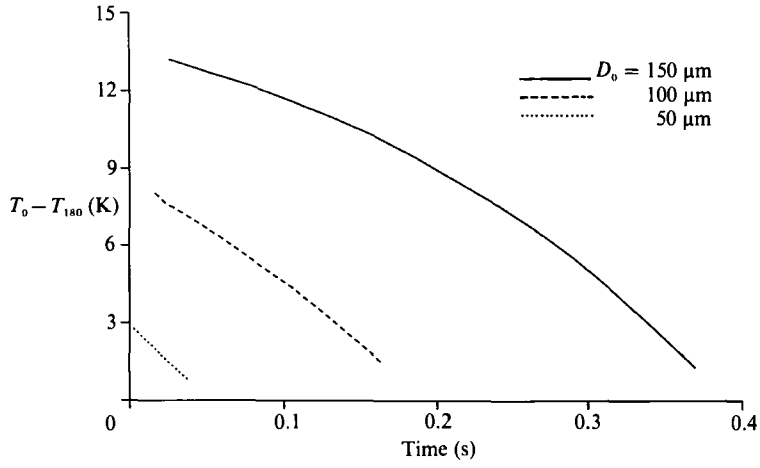

FIGURE 15. Temporal variation of the maximum temperature difference across the droplet surface for water droplets of different size (T_w = 673 K).

droplet sizes typically found in industrial sprays (less than 150 μm in diameter). The experimental work available in the literature has presented results for sessile drops 1–5 mm in diameter. Therefore, quantitative comparison has not been possible, since for such large drops, the sphericity assumption of the present study is not satisfied and the error due to linearization of Clausius–Clapeyron equation would be significant. Future work to extend and improve the present analysis should include the inertia terms in the conservation equations and the Clausius–Clapeyron equation without linearization so that the restrictions on the Reynolds number and on the droplet sizes considered can be lessened.

The authors are very grateful for the support of this research by the National Science Foundation through grant No. CBT-8707860 and by the Rutgers University Research Council Program.

Appendix A. Flow-field solution

The velocity components are given by

$$V_\xi = -\frac{3}{2}\frac{(\cosh\xi-\mu)^{-\frac{1}{2}}}{c^2}\sum_{n=-1}^{\infty} F_n(\xi)\,C_{n+1}^{-\frac{1}{2}}(\mu)+\frac{(\cosh\xi-\mu)^{\frac{1}{2}}}{c^2}\sum_{n=0}^{\infty} F_n(\xi)\,P_n(\mu) \qquad \text{(A 1)}$$

and

$$V_\eta = -\frac{(1-\mu^2)^{-\frac{1}{2}}}{c^2}(\cosh\xi-\mu)^{-\frac{1}{2}}\sum_{n=-1}^{\infty} C_{n+1}^{-\frac{1}{2}}(\mu)\,W_n(\xi), \qquad \text{(A 2)}$$

where

$$W_n(\xi) = \cosh\xi\frac{\mathrm{d}F_n(\xi)}{\mathrm{d}\xi}-\tfrac{3}{2}\sinh\xi F_n(\xi)-\frac{n}{2n+3}\frac{\mathrm{d}F_{n+1}(\xi)}{\mathrm{d}\xi}-\delta_n^{-1}\frac{n+1}{2n-1}\frac{\mathrm{d}F_{n-1}(\xi)}{\mathrm{d}\xi},$$

$\delta_n^{-1} = 0$ for $n = -1$ and $\delta_n^{-1} = 1$ for $n \neq -1$. Equations (A 1) and (A 2) are examined for singular points. For V_ξ, the only singular point could be at infinity ($\xi = 0, \mu = 1$). For V_η, the possible singular points are at infinity ($\xi = 0, \mu = 1$) and along the line of symmetry ($\mu = 1$ and $\mu = -1$). Next we consider these points in detail.

Consider first the possible singular point of V_ξ. Only the first term in (A 1) is singular at infinity ($\xi = 0, \mu = 1$). Since for $n \geqslant 1$, $C_{n+1}^{-\frac{1}{2}}(\mu) = (1-\mu^2) f(\mu)$ with $f(\mu)$ finite at $\mu = 1$, only terms for $n = -1$ and $n = 0$ in (A 1) are singular. The singularity is removed by requiring that

$$\lim_{\substack{\xi \to 0 \\ \mu \to 1}} \sum_{n=-1}^{0} F_n(\xi) C_{n+1}^{-\frac{1}{2}}(\mu) = 0.$$

This leads to

$$A_{-1} + C_{-1} = A_0 + C_0. \tag{A 3}$$

Next, we consider the singular points of V_η.

(i) Possible singularity at infinity ($\xi \to 0, \mu = 1$). Taking the limit as $\xi \to 0$ and $\mu = 1$ reveals that this point is not singular. Therefore, no requirement is imposed on the coefficients of the stream-function solution.

(ii) Along the line of symmetry ($\mu = 1$ and $\mu = -1$). Since for $n \geqslant 1$,

$$C_{n+1}^{-\frac{1}{2}}(\mu) = (1-\mu^2) f(\mu)$$

with $f(\mu)$ finite at $\mu = \pm 1$, only terms for $n = -1$ and $n = 0$ in (A 2) are singular. The singularity is removed by requiring that

$$\sum_{n=-1}^{0} C_{n+1}^{-\frac{1}{2}}(\mu) W_n(\xi) = 0,$$

for $\mu = \pm 1$. Then we have

$$W_{-1}(\xi) - W_0(\xi) = 0 \tag{A 4}$$

and

$$W_{-1}(\xi) + W_0(\xi) = 0. \tag{A 5}$$

Equations (A 4) and (A 5) lead to the following relations:

$$A_{-1} = \tfrac{1}{3} C_{-1} \tag{A 6}$$

$$B_{-1} = \tfrac{1}{3} D_{-1} \tag{A 7}$$

$$C_0 = \tfrac{1}{3} A_0 \tag{A 8}$$

and

$$D_0 = \tfrac{1}{3} B_0. \tag{A 9}$$

Letting $A_0 = A$, $D_{-1} = B$, $3D_0 = C$, and using (A 3) and (A 6)–(A 9), the stream function Ψ is given by

$$\Psi = (\cosh\xi - \mu)^{-\frac{3}{2}} \{ A(1-\mu)(\cosh \tfrac{1}{2}\xi + \tfrac{1}{3}\cosh \tfrac{3}{2}\xi) + (B + C\mu)(\sinh \tfrac{1}{2}\xi - \tfrac{1}{3}\sinh \tfrac{3}{2}\xi) + \sum_{n=1}^{\infty} F_n(\xi) C_{n+1}^{-\frac{1}{2}}(\mu) \}. \tag{A 10}$$

From physical considerations we set $B = C$, unless $V_\eta \neq 0$ along the z-axis.

Appendix B. Determination of coefficients in the flow-field solution

The integration constants A_n, B_n and B of the stream function Ψ are obtained by solving the following system of equations:

$$\delta_{n1} B(\cosh \tfrac{1}{2}\beta - \cosh \tfrac{3}{2}\beta) - \delta_n^1 \frac{n+1}{2n-1} [r_{n-1}(\beta) A_{n-1} + s_{n-1}(\beta) B_{n-1}] + [r_n(\beta)\cosh\beta - \tfrac{3}{2} p_n(\beta)\sinh\beta] A_n + [s_n(\beta)\cosh\beta - \tfrac{3}{2} q_n(\beta)\sinh\beta] B_n - \frac{n}{2n+3} [r_{n+1}(\beta) A_{n+1} + s_{n+1}(\beta) B_{n+1}] = 0, \quad n = 1, 2, \ldots \tag{B 1}$$

and $$\frac{2}{3c}H_n(\beta) = R_n(\beta)+S_n(\beta), \quad n = 0,1,2,\ldots. \tag{B 2}$$

In the above system of equations

$$p_n(\xi) = \cosh(n-\tfrac{1}{2})\xi - \cosh(n+\tfrac{3}{2})\xi, \tag{B 3}$$

$$q_n(\xi) = \sinh(n-\tfrac{1}{2})\xi - \frac{2n-1}{2n+3}\sinh(n+\tfrac{3}{2})\xi, \tag{B 4}$$

$$r_n(\xi) = (n-\tfrac{1}{2})\left[\sinh(n-\tfrac{1}{2})\xi - \frac{2n+3}{2n-1}\sinh(n+\tfrac{3}{2})\xi\right], \tag{B 5}$$

$$s_n(\xi) = (n-\tfrac{1}{2})[\cosh(n-\tfrac{1}{2})\xi - \cosh(n+\tfrac{3}{2})\xi], \tag{B 6}$$

$$\begin{aligned} H_n(\xi) = {} & (\sinh\tfrac{1}{2}\xi - \tfrac{1}{3}\sinh\tfrac{3}{2}\xi)[\delta_{n0}B(\tfrac{3}{2}+\cosh\xi)+\tfrac{1}{2}\delta_{n1}B] \\ & + \frac{2n+5}{2(2n+3)}F_{n+1}(\xi) + \frac{2n-3}{2(2n-1)}F_{n-1}(\xi) - \cosh\xi F_n(\xi), \end{aligned} \tag{B 7}$$

$$R_n(\xi) = \tfrac{1}{3}\sinh\xi\left\{\frac{n+1}{2n+3}G_{n+1}(\xi) + \frac{n}{2n-1}G_{n-1}(\xi) - \cosh\beta G_n(\xi)\right\}, \tag{B 8}$$

$$\begin{aligned} S_n(\xi) = {} & -\tfrac{2}{3}\cosh\xi^2\frac{\mathrm{d}G_n(\xi)}{\mathrm{d}\xi} + \tfrac{4}{3}\cosh\xi\left[\frac{n+1}{2n+3}\frac{\mathrm{d}G_{n+1}(\xi)}{\mathrm{d}\xi}\right. \\ & \left. + \frac{n}{2n-1}\frac{\mathrm{d}G_{n-1}(\xi)}{\mathrm{d}\xi}\right] - \frac{2}{3}\left[\frac{(n+1)(n+2)}{(2n+3)(2n+5)}\frac{\mathrm{d}G_{n+2}(\xi)}{\mathrm{d}\xi}\right. \\ & \left. + \frac{2n^2+2n-1}{(2n-1)(2n+3)}\frac{\mathrm{d}G_n(\xi)}{\mathrm{d}\xi} + \frac{n(n-1)}{(2n-1)(2n-3)}\frac{\mathrm{d}G_{n-2}(\xi)}{\mathrm{d}\xi}\right], \end{aligned} \tag{B 9}$$

and $$G_n(\xi) = c_n\frac{\sinh(n+\frac{1}{2})\xi}{\sinh(n+\frac{1}{2})\beta} - \lambda c_n\,\mathrm{e}^{-(n+\frac{1}{2})(\xi-\beta)}, \tag{B 10}$$

with $\lambda = \lambda_1/\lambda_g$. Also, $\delta_{ij}^{\prime} = 1-\delta_{ij}$, where δ_{ij} is the Kronecker delta function.

REFERENCES

Avedisian, C. T., Ioffredo, C. & O'Connor, M. J. 1984 Film boiling of discrete droplets of mixtures of coal and water on a horizontal brass surface. *Chem. Engng Sci.* **39**, 319–327.

Avedisian, C. T. & Koplik, J. 1987 Leidenfrost boiling of methanol droplets on hot porous/ceramic surfaces. *Intl J. Heat Mass Transfer* **30**, 379–393.

Gaunt, J. A. 1929 The triplets of helium. *Phil. Trans. R. Soc. Lond.* A **228**, 192–196.

Goldman, A. J., Cox, R. G. & Brenner, H. 1966 The slow motion of two identical arbitrarily oriented spheres through a viscous fluid. *Chem. Engng Sci.* **21**, 1151–1170.

Goldshtik, M. A., Khanin, V. M. & Ligai, V. G. 1986 A liquid drop on an air cushion as an analogue of Leidenfrost boiling. *J. Fluid Mech.* **166**, 1–20.

Gottfried, B. S. & Bell, K. J. 1966 Film boiling of spheroidal droplets. *Indust. Engng Chem. Fundam.* **5**, 561–568.

Gottfried, B. S., Lee, C. J. & Bell, K. J. 1966 The Leidenfrost phenomenon: film boiling of liquid droplets on a flat plate. *Intl J. Heat Mass Transfer* **9**, 1167–1187.

Haber, S., Hetsroni, G. & Solan, A. 1973 On the low Reynolds number motion of two droplets. *Intl J. Multiphase Flow* **1**, 57–71.

Law, C. K. 1982 Recent advances in droplet vaporization and combustion. *Prog. Energy Combust. Sci.* **8**, 171–201.

MICHIYOSHI, I. & MAKINO, K. 1977 Heat transfer characteristics of evaporation of a liquid droplet on heated surfaces. *Intl J. Heat Mass Transfer* **21**, 605–613.

NGUYEN, T. K. & AVEDISIAN, C. T. 1987 Numerical solution for film evaporation of a spherical liquid droplet on an isothermal and adiabatic surface. *Intl J. Heat Mass Transfer* **30**, 1497–1509.

OGUZ, H. N. & SADHAL, S. S. 1987 Growth and collapse of translating compound multiphase drops: analysis of fluid mechanics and heat transfer. *J. Fluid Mech.* **179**, 105–136.

RAZNJEVIC, K. 1976 *Handbook of Thermodynamic Tables and Charts*. Hemisphere.

SADHAL, S. S. & OGUZ, H. N. 1985 Stokes flow past compound multiphase drops: the case of completely engulfed drops/bubbles. *J. Fluid Mech.* **160**, 511–529.

SAMPSON, R. A. 1891 On Stokes's current function. *Phil. Trans. R. Soc. Lond.* A **182**, 449–518.

SEN, A. K. & LAW, C. K. 1984 On a slowly evaporating droplet near a hot plate. *Intl J. Heat Mass Transfer* **27**, 1418–1421.

STIMSON, M. & JEFFERY, G. B. 1926 The motion of two spheres in a viscous fluid. *Proc. R. Soc. Lond.* A **111**, 110–116.

TAMURA, Z. & TANASAWA, Y. 1959 Evaporation and combustion of a drop contacting with a hot surface. In *Seventh Intl Symp. on Combustion*, pp. 509–522. Butterworths.

VARGAFTIK, N. B. 1975 *Handbook of Physical Properties of Liquids and Gases*. Hemisphere.